nature communications

Article

https://doi.org/10.1038/s41467-025-64331-z

Martian differentiation history inferred from copper isotopes

Received: 29 November 2024

Accepted: 15 September 2025

Published online: 21 October 2025

Check for updates

De-Liang Wang[1,2], Dan Zhu[3,4], Ying-Kui Xu[1,4] ✉, Shui-Jiong Wang[5,6], Shi-Jie Li[1,4] ✉, Zi-Ru Liu[5], Yang Li[1,4], Zhi Li[1,2], Hong Tang[1,4], Xiong-Yao Li[1,4] & Jian-Zhong Liu[1,4]

Sulfide segregation plays an important role in redistributing chalcophile elements during planetary differentiation, yet its efficiency on Mars remains poorly constrained. Here, we report the Cu isotopic evidence for planetary-scale sulfide segregation during martian differentiation. We find that the bulk silicate Mars exhibits a measurable enrichment in isotopically heavy Cu ($\delta^{65}Cu_{BSMa} = -0.03 \pm 0.08‰$, 2 SD) compared with its chondritic precursors ($\delta^{65}Cu = -0.30 \pm 0.09‰$). This isotopic offset cannot be explained by magma ocean devolatilization alone and instead requires preferential incorporation of isotopically light Cu into the core via sulfide segregation. A two-stage core formation model, constrained by established martian building blocks, yields an upper limit for mantle sulfur (400–443 μg/g) with corresponding copper (6–8 μg/g) abundances. These values are consistent with previous estimates for a sulfur-poor martian mantle, as such a mantle facilitates the generation of S-undersaturated melts. Our model further supports a sulfur-rich martian core (~16.1 wt.% S and ~354 μg/g Cu). These findings identify sulfide segregation as a key control on Cu isotopic compositions and chalcophile element budgets during planetary differentiation, providing constraints on Mars' early evolution.

A significant unresolved constraint on martian planetary differentiation is the efficiency of sulfide segregation. This process fundamentally controls martian chalcophile element budgets, such as sulfur (S) and copper (Cu). However, we currently lack robust constraints on sulfide segregation during martian differentiation derived from martian samples. Although evidence from silver (Ag) partitioning systematics in high-pressure experiments suggests limited sulfide segregation on Mars[1], this inference requires robust validation. Copper isotopes ($\delta^{65}Cu$) provide a powerful tracer to address this knowledge gap. Specifically, sulfide–silicate partitioning induces significant equilibrium Cu isotopic fractionation, as Ni-poor sulfides preferentially incorporate isotopically light Cu[2,3]. This significant fractionation contrasts with the minimal fractionation ($\Delta^{65}Cu_{metal\text{-}silicate}$ about +0.1‰ to +0.2‰[2,3]) characteristic of high-temperature metal–silicate equilibration associated with core formation. Therefore, $\delta^{65}Cu$ serves as a highly diagnostic indicator of sulfide-dominated processes.

Current constraints on the Cu isotopic composition of bulk silicate Mars (BSMa) remain limited. Existing constraints on martian $\delta^{65}Cu$ rely on a single measurement ($\delta^{65}Cu = -0.15‰$ for a shergottite melt glass[4]), which is insufficient to represent the BSMa. Therefore, determining the BSMa $\delta^{65}Cu$ will allow comparative planetology to assess whether martian differentiation proceeded similarly to that of Earth

[1]Center for Lunar and Planetary Sciences, Institute of Geochemistry, Chinese Academy of Sciences, Guiyang, China. [2]University of Chinese Academy of Sciences, Beijing, China. [3]State Key Laboratory for Critical Mineral Research and Exploration, Institute of Geochemistry, Chinese Academy of Sciences, Guiyang, China. [4]CAS Center for Excellence in Comparative Planetology, Hefei, China. [5]State Key Laboratory of Geological Processes and Minerals Resources, China University of Geosciences (Beijing), Beijing, China. [6]Frontiers Science Center for Deep-time Digital Earth, China University of Geosciences (Beijing), Beijing, China. ✉e-mail: xuyingkui@vip.gyig.ac.cn; lishijielpsc@mail.gyig.ac.cn

https://doi.org/10.1038/s41467-025-64331-z

Table 1 | Copper isotopic compositions of the measured samples and geological reference materials

Group	Subtype	Name	δ^{65}Cu (‰)	2 SD (‰)[g]	N[h]
Shergottite	Basaltic	NWA 12269	−0.01	0.05	3
		NWA 12594	0.02	0.05	3
		NWA 12594 repeat	0.01	0.05	3
		NWA 2975	0.12	0.05	3
		NWA 8657	−0.07	0.05	3
		Zagami	−1.19	0.06	3
		Zagami chip 2	−1.00	0.06	3
		NWA 12564	0.01	0.05	3
		NWA 12564 chip 2	0.04	0.05	3
		NWA 12564 chip 2 repeat	0.05	0.05	3
		NWA 13327	−0.07	0.05	3
		Swayyah 002	−0.08	0.05	3
		Swayyah 002 repeat	−0.05	0.05	3
	Gabbroic	NWA 6963	0.63	0.06	3
		NWA 6963 chip 2	0.49	0.06	3
	Olivine-phyric	NWA 1068	−0.12	0.05	3
	Poikilitic	NWA 7397	−0.29	0.06	3
		NWA 13276	0.00	0.05	3
		NWA 13276 chip 2[a]	0.02	0.06	3
		NWA 13367	−0.03	0.05	3
		NWA 13367 chip 2	−0.04	0.05	3
Nakhlite	Augite-olivine-rich	Qued Mya 005	−0.06	0.05	3
		Qued Mya 005 chip 2	−0.15	0.06	3
		NWA 10645	−0.44	0.06	3
Reference material	Basalt	BHVO-2	0.06	0.05	3
			0.03	0.06	3
			0.07[b]	0.06	–
			0.08[c]	0.05	–
			0.10[d]	0.05	–
			0.12[e]	0.02[e]	–
		BIR-1a	0.02	0.05	3
			0.02[f]	0.04	–
			0.02[e]	0.06[e]	–
	Peridotite	JP-1	0.06	0.05	3
			0.03[f]	0.05	–

[a]Weathered exterior of NWA 13276 chip 1, excluded from the average.
[b]Day et al.[13].
[c]Ni et al.[12].
[d]Huang et al.[15].
[e]Moynier et al.[96], uncertainty is expressed as 2 SE (twice the standard error).
[f]Liu et al.[5].
[g]Uncertainties for measured samples are reported as 2 SD (twice the standard deviation of standard solution analyses during an analytical session).
[h]Number of measurements per sample solution.

and the Moon, or whether it followed a distinct pathway. Insights from the isotopic signatures of Earth and the Moon underscore this importance. Published data indicate that the bulk silicate Earth (BSE) exhibits δ^{65}Cu values of +0.07 ± 0.10‰[2] and +0.06 ± 0.20‰[5], which are indistinguishable within uncertainties. These values are constrained through analyses of diverse terrestrial igneous suites, including mid-ocean ridge basalts (MORBs), ocean island basalts (OIBs), komatiites, and peridotites[2,5]. Herein, we adopt the δ^{65}Cu value of +0.07 ± 0.10‰ owing to its lower uncertainty. This lower uncertainty arises because the value includes komatiites rather than peridotites, as the latter are more susceptible to alteration and possess complex petrogenetic histories. The BSE exhibits a heavy δ^{65}Cu signature relative to its modeled bulk composition, supporting substantial sulfide segregation during differentiation[2]. Similarly, the bulk silicate Moon (BSMo) δ^{65}Cu value is significantly higher, at +0.57 ± 0.15‰, as constrained by low-Ti basalts[6]. Additionally, local metal–silicate equilibration and metal trapping in mantle cumulates may have caused heterogeneity within the lunar mantle during solidification of the lunar magma ocean[7], adding complexity to the interpretation of the BSMo signature. The δ^{65}Cu value of BSMo exceeds that of chondrites[2,6,8–11]. However, the origin of the elevated BSMo δ^{65}Cu value is debated, as two distinct processes could explain the removal of isotopically light Cu from the silicate reservoir: sulfide segregation[2,3] versus devolatilization[12,13]. Paquet et al.[6] suggested that volatile loss induced the isotopically heavy Cu signature in BSMo, whereas Xia et al.[3] attributed this signature predominantly to sulfide segregation. This highlights the challenge in uniquely assigning δ^{65}Cu variations to specific processes and emphasizes the non-negligible role of volatile loss.

To address the knowledge gap regarding the δ^{65}Cu of the BSMa and to quantify the effects of sulfide segregation during martian differentiation, we present a Cu isotopic dataset for a diverse suite of martian meteorites (13 shergottites and 2 nakhlites). By integrating these data with a revised differentiation model, we: (1) constrain the δ^{65}Cu of the BSMa; (2) assess the relative contributions of sulfide segregation versus volatile loss to the BSMa's Cu isotopic signature; and (3) constrain S-Cu co-evolution during martian magma ocean (MMO) crystallization. This study provides important isotopic evidence to help resolve the martian sulfide segregation issue and advances our understanding of martian core–mantle differentiation and chalcophile budgets.

Results and discussion

Chemical and copper isotopic compositions of martian meteorites

To provide petrographic context, features of the measured martian meteorites are detailed in Supplementary Note 1 and Supplementary Figs. 1–11. Chemical compositions are detailed in Supplementary Data 1. Measured δ^{65}Cu values for the martian meteorites are summarized in Table 1 and Fig. 1. Analytical accuracy was confirmed using geological reference materials (BHVO-2, BIR-1a, and JP-1), and the measured δ^{65}Cu values for these reference materials are consistent with published reference data (Table 1). Isotopic analyses ($n = 6$) of multiple fragments from individual meteorites revealed consistent δ^{65}Cu values. Heterogeneities exceeding analytical uncertainty were observed in limited instances ($n = 2$), potentially attributable to the nugget effect in coarse-grained gabbro (e.g., Northwest Africa (NWA) 6963) and the anomalous shergottite Zagami. Furthermore, no measurable Cu isotopic variation was observed between the weathered exterior and less altered interior of NWA 13276, confirming that terrestrial weathering did not significantly alter the Cu isotopic composition.

Shergottites exhibit a broad range of δ^{65}Cu values, from −1.19‰ (Zagami) to +0.63‰ (NWA 6963). Given their extreme values relative to other shergottites, Zagami and NWA 6963 are identified as outliers and excluded from further analysis of the dominant shergottite group. The remaining shergottites ($n = 11$) define a narrower δ^{65}Cu range from −0.29‰ to +0.12‰, with a mean value of −0.05 ± 0.21‰ (2 SD). Within this shergottite group (excluding outliers), a correlation is observed between δ^{65}Cu values and their established geochemical classification:

https://doi.org/10.1038/s41467-025-64331-z

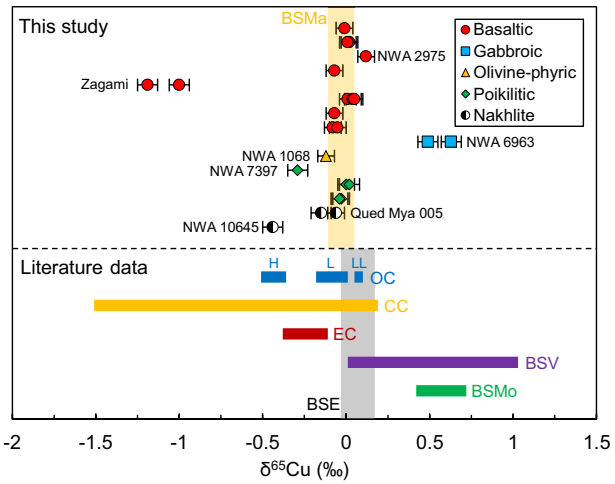

Fig. 1 | Copper isotopic compositions of celestial reservoirs. Error bars represent 2 SD (based on the precision of standard solutions applied to samples). Chondritic δ^{65}Cu ranges, including ordinary chondrite (OC), carbonaceous chondrite (CC), and enstatite chondrite (EC), are compiled from the literature[2,8–11]. Compiled δ^{65}Cu values are compared with bulk silicate Earth (BSE, defined by MORBs, OIBs, komatiites, and peridotites[2]), bulk silicate Moon (BSMo, defined by lunar basalts[6]), and bulk silicate Vesta (BSV, defined by eucrites[48]).

intermediate shergottites ($0.3 < (La/Yb)_{CI} < 0.8$[14]) versus enriched shergottites ($(La/Yb)_{CI} > 0.8$[14]) (Fig. 2a). The two nakhlites analyzed yielded δ^{65}Cu values of −0.44‰ to −0.06‰, both lower than the mean value (−0.05‰) of the dominant shergottite group.

Copper isotopic fractionation during magmatic processes

Martian meteorites exhibit resolvable δ^{65}Cu variations (Fig. 1). Zagami and NWA 6963 were excluded from consideration due to potential non-magmatic alteration or contamination (Supplementary Discussion 1). Similar to terrestrial systems where high-degree mantle melting induces limited Cu isotopic fractionation[2,5,15], sulfide-dominated processes likely dominate Cu isotopic fractionation during martian magmatism. This dominance stems from sulfides' important role in controlling Cu partitioning during peridotite melting[16] and preserving siderophile/chalcophile signatures in shergottites[17,18]. Therefore, sulfide-undersaturated magmas lacking sulfide segregation have the potential to preserve mantle-derived Cu isotopic compositions. Evidence for sulfide saturation processes is recorded in geochemical indicators. Specifically, sulfide-undersaturated magmas exhibit incompatible Cu behavior, with concentrations increasing systematically during magmatic evolution[19] (Fig. 2b). In contrast, samples like NWA 2975 exhibit anomalous Cu depletion coupled with heavy δ^{65}Cu (Fig. 2a, b), indicating having undergone sulfide segregation. This sulfide saturation is linked to NWA 2975's anomalously low FeO content (17 wt.% versus 19–24 wt.% in other analyzed shergottites), as sulfur content at sulfide saturation (SCSS) decreases with decreasing melt FeO content[20,21]. The Cu/Zr ratio remains stable during sulfide-absent melting and early-stage mafic magma differentiation but is sensitive to sulfide segregation events[22]. Consequently, the lack of Cu/Zr-MgO correlation in shergottites (Supplementary Fig. 12) suggests the absence of widespread sulfide segregation. Most samples cluster at $Cu/Zr \approx 0.3–0.4$, consistent with this interpretation. However, elevated ratios in olivine-phyric and poikilitic shergottites likely reflect nugget effects (Supplementary Discussion 2), rather than sulfide segregation processes. Collectively, these observations indicate that martian mantle-derived melts are dominantly sulfide-undersaturated.

However, MMO differentiation produces a heterogeneous martian mantle, as recorded by incompatible trace element (ITE) systematics (e.g., rare earth element (REE) patterns, ^{87}Rb-^{86}Sr, ^{147}Sm-^{144}Nd, and ^{176}Lu-^{177}Hf) of shergottites[23–27]. ITE-depleted signatures reflect early cumulates, whereas ITE-enriched signatures are preserved in mantle domains formed by the crystallization of late-stage melts[23–27]. The residence of ITE-depleted reservoirs in the mantle is broadly accepted, but the source of ITE-enriched reservoirs remains debated. In particular, some studies propose the martian crust as a possible ITE-enriched reservoir[28,29]. Despite uncertainty in the specific mechanism, the covariation between δ^{65}Cu and $(La/Yb)_{CI}$ (Fig. 2a) indicates that isotopically light Cu signatures associate with ITE-enriched components. This coupling may reflect complex magma evolution concentrating isotopically light Cu within ITE-enriched mantle domains. Alternatively, it could indicate that the lower crust is the ITE-enriched source of shergottites. Support for the latter scenario comes from terrestrial analogs, which show that late-stage crystallization of basaltic magmas in lower crust generates isotopically light Cu signatures through sulfide enrichment in mafic cumulates[30–32]. Therefore, mixing between isotopically light Cu reservoirs (e.g., ITE-enriched mantle domains or lower crust) and ITE-depleted mantle sources could generate the observed ITE-δ^{65}Cu covariation.

To trace the effects of sulfide segregation and mixing with an ITE-enriched reservoir, we utilize Ni/Co and $(La/Yb)_{CI}$ ratios. These proxies co-vary during silicate-dominated processes (e.g., fractional crystallization and partial melting) but decouple under secondary mechanisms. The Ni/Co systematics reveal key constraints. Nickel and cobalt are compatible in olivine/pyroxene, with Ni being more compatible[33], leading to Ni depletion in residual melts and a strong MgO-Ni/Co correlation (Fig. 2c). This correlation and bulk Ni/Co <6 preclude significant meteoritic contamination (bulk Ni/Co ≥20 in chondrites and iron meteorites[34]). Regarding the $(La/Yb)_{CI}$ proxy, ratios increase during magmatic evolution as La is more incompatible than Yb. Notably, decoupling between Ni/Co and $(La/Yb)_{CI}$ (Fig. 2d) reveals distinct secondary processes. Specifically, sulfide segregation preferentially depletes Ni owing to its stronger chalcophile affinity relative to Co[35], thereby reducing Ni/Co ratios below values expected from silicate-dominated trend (e.g., NWA 2975). For assimilation of ITE-enriched reservoirs, this process elevates $(La/Yb)_{CI}$ values but minimally affects Ni/Co ratios due to the reservoirs' relatively low Ni and Co concentrations, inherited from MMO late-stage melts or the lower crust. Consequently, assimilation amplifies REE pattern variations while preserving primordial Ni/Co (e.g., NWA 1068 and NWA 7397). Overall, this diagnostic framework reveals three principal processes governing shergottite Cu isotopic fractionation (Fig. 2d). First, silicate-dominated processes yield uniform δ^{65}Cu values (-0.03 ± 0.08‰), reflecting the mantle pristine signature. Second, under reducing conditions, segregation of Ni-poor sulfide melts preferentially removes isotopically light Cu[2,3,36], resulting in residual silicate melts enriched in heavier Cu isotopes (e.g., NWA 2975). Third, mixing with ITE-enriched reservoirs induces isotopic variability (e.g., NWA 1068 and NWA 7397). Consequently, Cu isotopic variability in shergottites is dominantly controlled by sulfide saturation history and mixing between distinct mantle sources during martian magmatism.

Regarding nakhlites, these cumulate-rich rocks originate from low-degree melting of ITE-depleted mantle sources[37–40], yet exhibit characteristics of aqueous alteration (e.g., iddingsite[41]) and potential crustal contamination[37]. Nakhlites exhibit lower δ^{65}Cu values than most shergottites (Fig. 1), implying contributions from ITE-enriched components or alteration effects. However, the limited nakhlite dataset ($n = 2$, with measurable δ^{65}Cu variations) precludes robust conclusions. The isotopic difference between shergottites and nakhlites likely reflects differences in melt extraction degree (high- versus low-degree partial melting) and/or post-magmatic alteration, highlighting the need for expanded nakhlite Cu isotopic analyses.

https://doi.org/10.1038/s41467-025-64331-z

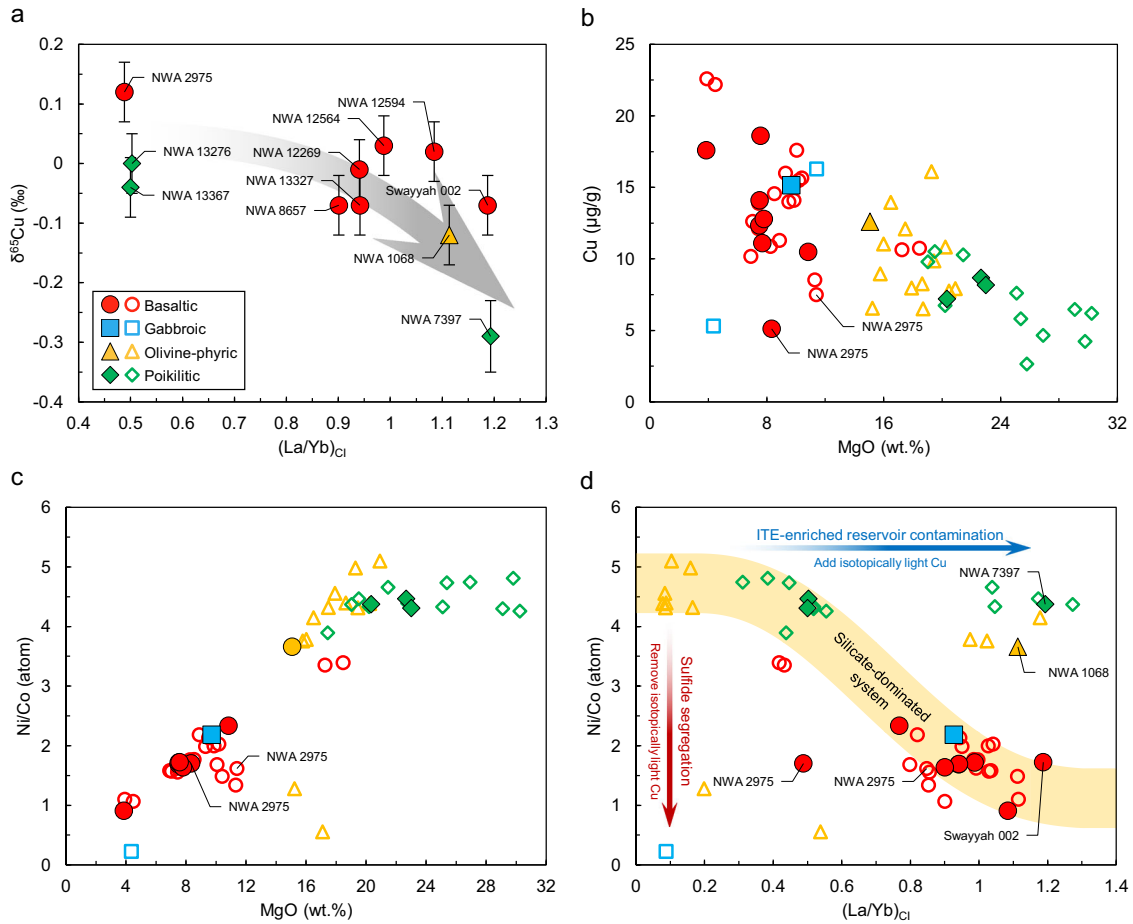

Fig. 2 | Isotope and element systematics in shergottites. Solid symbols represent data from this study, and open symbols denote literature data from Wang and Becker[19] and the data compilation by Udry et al. [14]. The complete compiled dataset is provided in Supplementary Data 5. A unified legend applies to all panels. Error bars represent 2 SD (based on the precision of standard solutions applied to samples). Uncertainties for the mean values of replicate samples are assigned as the maximum of these 2 SD values. CI chondrite reference values are from Sun and McDonough[97]. **a** δ^{65}Cu and $(La/Yb)_{CI}$ exhibit a negative correlation. **b** Cu and MgO contents show a negative correlation in most shergottites. **c** Ni/Co ratios and MgO contents display a positive correlation. **d** Ni/Co versus $(La/Yb)_{CI}$ categorizes shergottites into three evolutionary groups: silicate-dominated, sulfide segregation, and ITE-enriched reservoir contamination. The orange-shaded field denotes the proposed silicate-dominated trend.

Copper isotopic composition of BSMa and bulk Mars

The identification of sulfide segregation and mixing with ITE-enriched reservoirs as principal controls on shergottite δ^{65}Cu variations enables the constraint of the pristine Cu isotopic composition of the BSMa. This requires isolating samples preserving the pristine mantle-derived signatures, minimizing influences from both secondary alteration and significant magmatic modification. To ensure robust statistics and equal weighting among meteorites, δ^{65}Cu values for shergottites with multiple subsamples (e.g., NWA 12594, NWA 12564, NWA 13367) were averaged prior to screening. This approach prevents over-representation of individual meteorites with more replicates in subsequent analyses.

To isolate the pristine mantle signature, we employed a two-step screening protocol. First, we focused on removing meteorites affected by non-magmatic processes to establish a dataset documenting igneous processes. Samples showing characteristics of non-magmatic alteration (Zagami, NWA 6963) or potential aqueous alteration/crustal contamination (Qued Mya 005, NWA 10645) were excluded. This initial filtering yielded eleven meteorites interpreted as mantle-derived melts recording magmatic effects, exhibiting δ^{65}Cu values ranging from −0.29‰ to +0.12‰ (mean: −0.05 ± 0.21‰, 2 SD). Subsequently, a second distinct screening step was applied to this group of eleven meteorites to specifically target and minimize the influence of magmatic processes, thereby isolating the signature of the pristine martian mantle. Meteorites exhibiting geochemical signatures of sulfide segregation (NWA 2975) and strong contributions from ITE-enriched reservoir mixing (NWA 7397, NWA 1068) were excluded. This two-step screening resulted in a final suite of eight meteorites that represent the unmodified Cu isotopic composition of the BSMa. The $\delta^{65}Cu_{BSMa}$ value is thus defined by the mean of these eight averaged compositions, yielding −0.03 ± 0.08‰ (2 SD). In particular, this BSMa composition is slightly lower than, but overlaps within uncertainty with, the BSE estimate of +0.07 ± 0.10‰[2] (Fig. 1).

Quantitative modeling of martian differentiation requires knowledge of the bulk Mars composition ($\delta^{65}Cu_{BM}$). However, significant δ^{65}Cu heterogeneity among chondrite groups[2,8–11] (Fig. 1 and Supplementary Data 2) reflects primordial diversity in planetary building blocks, necessitating model-dependent assumptions regarding Mars' accretionary components. Previous oxygen isotope-based accretion models proposed distinct mixtures: Lodders and Fegley[42] proposed 4% CI, 11% CV, and 85% H chondrites, while Sanloup et al. [43] estimated 45% EH and 55% H chondrites. Recent isotopic evidence[44–47] supports limited carbonaceous chondrite contributions (<6%), consistent with the model proposed by Sanloup et al.[43]. Using this preferred accretion model and incorporating chondritic Cu abundances and isotopic data[2,8,11], our mass balance calculation yields a $\delta^{65}Cu_{BM}$ of

https://doi.org/10.1038/s41467-025-64331-z

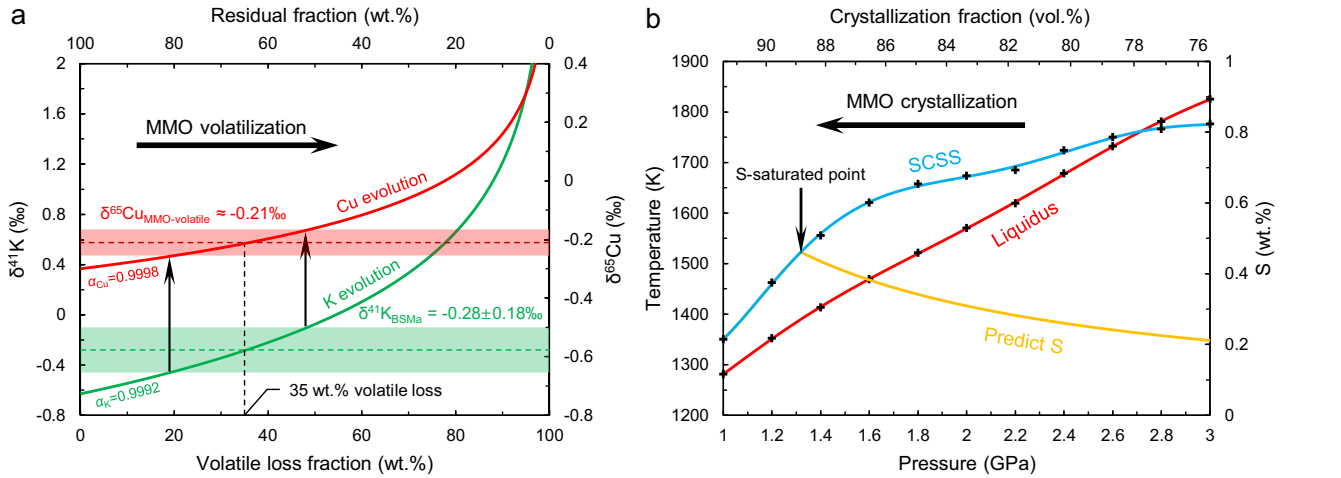

Fig. 3 | Martian magma ocean (MMO) evolutionary signatures during devolatilization and crystallization. a Copper and potassium isotope systematics reveal distinct fractionation extents. Potassium isotopes ($\delta^{41}K$) exhibit greater fractionation than Cu isotopes ($\delta^{65}Cu$) at equivalent volatile loss fraction. Rayleigh fractionation modeling (fractionation factors α from Sossi et al. [54]; Supplementary Method 2) indicates ~35% K depletion. Assuming analogous Cu volatility, $\delta^{65}Cu$ increases by 0.09‰. Value for $\delta^{41}K_{BSMa}$ follows Tian et al. [57], $\delta^{65}Cu$ and $\delta^{41}K$ of bulk Mars derive from mass balance calculations (Supplementary Method 1). **b** The alphaMELTS 1.9 simulations (0.2 GPa step size) reveal that the basal liquidus temperatures (in K) and the sulfur content at sulfide saturation (SCSS; in wt.%) decrease with MMO crystallization. Polynomial fits through discrete steps (black crosses) illustrate relationships between crystallization progress and residual melt properties. Predicted S contents (in wt.%) are calculated by mass balance, assuming full S retention in silicate melt until sulfide saturation. SCSS parameterization follows Blanchard et al. [21].

−0.30 ± 0.09‰ (Supplementary Method 1). The isotopic offset between the bulk Mars and BSMa compositions implies that isotopically light Cu was likely sequestered into the core or lost via evaporation during planetary differentiation.

Modeling S-Cu behavior during martian differentiation

To decipher the processes recorded in the Cu isotopic signature of BSMa, which serves as a key constraint on volatile depletion and core–mantle differentiation, we model S and Cu partitioning and isotopic fractionation. Three key stages influence $\delta^{65}Cu$ in the silicate reservoir: magma ocean devolatilization, metal segregation, and sulfide segregation. Magma ocean devolatilization enriches the silicate residue in isotopically heavy Cu, consistent with observations on the Moon[6] and Vesta[48]. Metal segregation preferentially incorporates isotopically heavy Cu into the iron alloy liquid, leaving an isotopically lighter silicate residue[2,3]. In contrast, sulfide segregation enriches the silicate reservoir in isotopically heavy Cu[2,3]. Quantitative modeling is required to distinguish these overlapping isotopic effects and quantify their net contribution to $\delta^{65}Cu_{BSMa}$.

The contribution of early volatile loss to the martian Cu isotopic composition was evaluated. Mars completed its primary accretion within 5 million years of calcium–aluminum-rich inclusion formation[49], while the nebular gas was still present[50]. During this stage, energy from giant impacts[51], rapid pebble accretion[52], and the radioactive decay of ^{26}Al[53] collectively caused global melting and volatile escape. Critically, the H_2-rich nebular atmosphere surrounding Mars significantly suppressed the extent of isotopic fractionation during evaporation[54]. Potassium (K) isotopes served as our proxy for Cu volatility. This approach is justified because: (1) both K and Cu exhibit similar depletion patterns in volatile-depleted, sulfur-poor bodies like the Moon[6]; and (2) K is lithophile, ensuring its isotopic signature reflects only volatile loss, and is unaffected by metal segregation or sulfide segregation events that influence Cu. Based on mass balance calculations (Supplementary Method 1) using a chondritic accretion model (45% EH and 55% H[43]) and end-member signatures (data from Wasson et al.[55] and the data compilation by Hu et al.[56]; Supplementary Data 2), the predicted bulk Mars $\delta^{41}K_{BM}$ is −0.63 ± 0.22‰. This contrasts sharply with the measured BSMa $\delta^{41}K_{BSMa}$ value ($\delta^{41}K_{BSMa}$ = −0.28 ± 0.18‰[57]). To reconcile this difference, Rayleigh fractionation modeling (Supplementary Method 2) constrained by previous work[54] under H_2-rich conditions was employed, using fixed fractionation factors of $\alpha_{Cu} = 0.9998$ and $\alpha_K = 0.9992$. Modeling results (Fig. 3a) indicate ~35% K depletion. Under the assumption of equivalent volatile loss fractions for Cu (based on their correlated volatile behavior), the resultant increase in $\delta^{65}Cu$ is 0.09‰, yielding $\delta^{65}Cu_{MMO\text{-}volatile} \approx -0.21‰$ (Fig. 3a). Consequently, volatile loss alone cannot explain the observed heavy $\delta^{65}Cu_{BSMa}$ signature.

Subsequently, the S-Cu behavior during core formation was quantified using a single-stage accretion and two-stage core formation model (adapted from O'Neill[58]), based on the accretion scenario of Sanloup et al. [43]. During the first stage (Fig. 4a), our model focused on metal segregation under the pressure (*P*) and temperature (*T*) conditions estimated for the final major equilibration event between the MMO and the iron alloy liquid. These conditions (~14 GPa and ~2100 K[59]) align with constraints from martian siderophile element systematics[59–61]. To determine the MMO composition during metal segregation, we performed mass balance calculations. These calculations incorporated experimentally determined metal–silicate partition coefficients for S[62] and Cu[63] (Supplementary Methods 3–5). This yielded initial MMO concentrations of ~515 µg/g S and ~10 µg/g Cu. Critically, the SCSS for initial MMO (~17.7 wt% FeO[43]) at 14 GPa and 2100 K is ~3666 µg/g (based on the parameterization by Blanchard et al.[21]; Supplementary Method 6). This SCSS value far exceeds the modeled S concentration, indicating sulfide undersaturation was maintained during metal segregation. Concurrently, iron alloy liquid incorporates isotopically heavy Cu ($\Delta^{65}Cu_{metal\text{–}silicate}$ about +0.1‰ to +0.2‰[2,3], with a conservatively adopted value of +0.1‰), and applying this fractionation reduces the $\delta^{65}Cu$ of the post-volatile MMO by 0.09‰ to −0.30‰. However, this modeled post-metal-segregation $\delta^{65}Cu$ is lighter than the observed BSMa value, revealing an isotopic discrepancy.

The isotopic discrepancy necessitates a process to enrich the silicate reservoir in isotopically heavy Cu. Although some models propose that S loss via degassing may be significant[64,65], others argue for S retention in planetary cores[66,67]. Owing to uncertainties in S evaporation efficiency, our model therefore focuses on late-stage sulfide segregation (the second stage of core formation) during magma ocean crystallization as the primary mechanism for S depletion in the silicate

https://doi.org/10.1038/s41467-025-64331-z

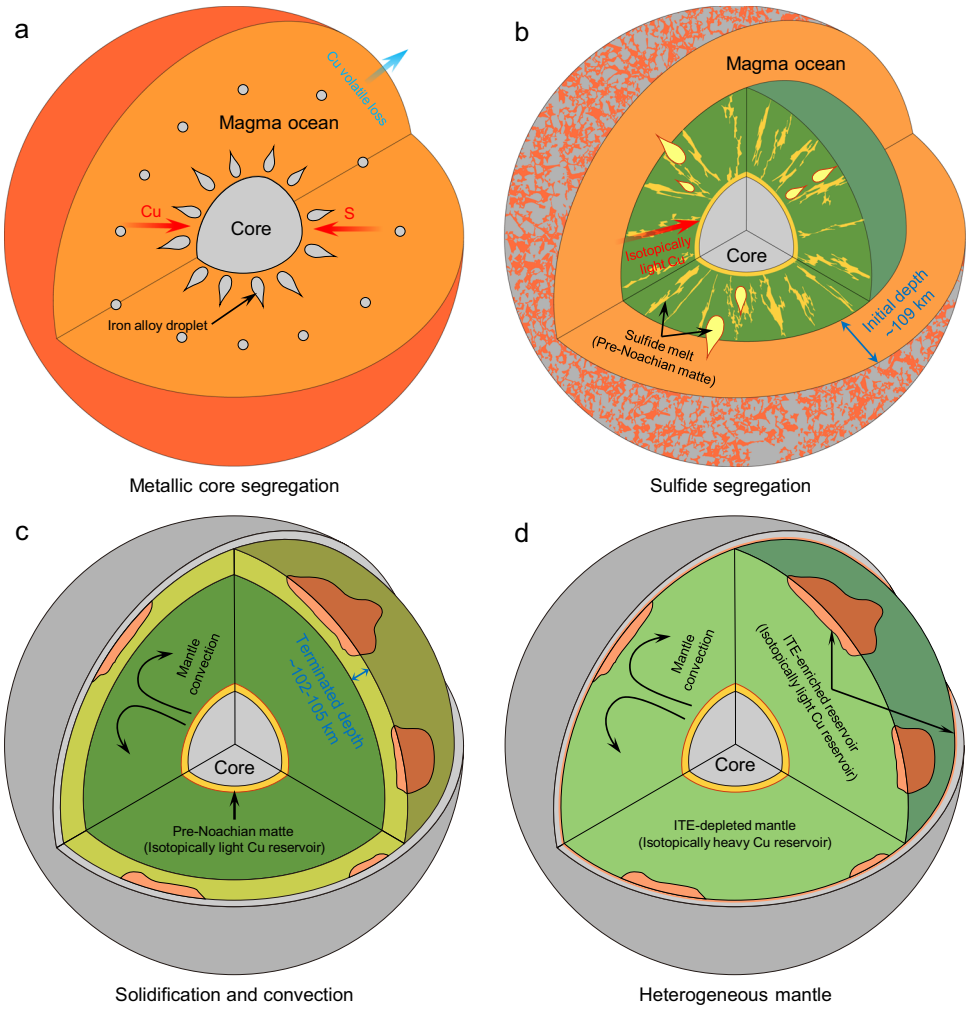

Fig. 4 | Schematic diagram of the proposed martian evolutionary model in this study. a Early core formation involved preferential sequestration of chalcophile elements into the metallic core (~16.1 wt.% S and ~345 μg/g Cu). The pre-metal segregation composition was modeled as a mixture of 45% EH and 55% H chondrites[43], with evaporated Cu subtracted (Fig. 3a). Partition coefficients of S and Cu followed literature parameterizations[62,63] (Supplementary Methods 3–5). **b** Progressive magma ocean crystallization triggered sulfide droplet exsolution (SCSS parameterized by Blanchard et al. [21]; Fig. 3b), with sulfide droplets subsequently percolating downward to the core. **c** The Pre-Noachian matte delivered a significant flux of chalcophile elements to the core. However, declining sulfide transport efficiency terminated this process. Final core concentrations (~16.1 wt.% S, ~354 μg/g Cu; mass balance calculation, this study) only minimally modified by subsequent minor S additions (~0.02% of the bulk core, far less than the pre-existing S). Residual melts enriched in ITEs formed ITE-enriched mantle domains that potentially retained isotopically light Cu. **d** Insufficient mantle convection produced a heterogeneous martian mantle, and ITE-enriched mantle domains or the lower crust may serve as reservoirs for isotopically light Cu.

reservoir. In the cooling and crystallizing magma ocean, sulfur concentrated in the residual melt. Concurrently, decreasing T–P and evolving MMO composition (constrained by alphaMELTS 1.9 simulation[68–70]; see Methods section for details) progressively reduced the SCSS[21,71], eventually triggering sulfide saturation (~89% crystallization, ~109 km depth; Fig. 3b). This sulfide segregation depth is consistent with independent estimates of a range of 40–320 km[72]. The resulting immiscible dense iron sulfide melts (i.e., Pre-Noachian matte, analogous to Earth's Hadean matte[58]; Fig. 4b) were enriched in isotopically light Cu ($\Delta^{65}Cu_{sulfide-silicate}$ about −0.80‰ to −0.89‰, parameterized by Xia et al.[3]) and began to percolate downward[73]. Critically, nickel depletion (<25 μg/g; Supplementary Method 7) in the residual melt, caused by olivine and/or pyroxene crystallization[33], enabled significant Cu isotopic fractionation[3]. Rayleigh fractionation modeling (Fig. 5a; Supplementary Method 7) incorporating Cu sulfide–silicate partitioning coefficients[74] and isotopic fractionation factors[3], constrained the isotopic composition of residual MMO to reach a $\delta^{65}Cu_{BSMa}$ value at the depth of 102–105 km. This depth represents the shallowest source region from which sulfide droplets can effectively reach the core.

At depths shallower than 102–105 km, lower geothermal temperatures suppressed further percolation of sulfide droplets into the core (Fig. 4c). Sulfide droplets exsolved at shallower depths may still percolate downward, but are unable to migrate sufficiently to reach the core (i.e., segregate from BSMa). Consequently, a portion of sulfide melts, enriched in isotopically heavy Cu relative to the bulk segregated sulfide (which is enriched in isotopically light Cu), was trapped within the crystallized magma ocean. These residual sulfides were subsequently redistributed by mantle overturn and convective mixing. This trapping mechanism enriched the BSMa in isotopically heavy Cu, thereby reconciling the modeled core formation result with the observed BSMa signature. Simultaneously, it established the primordial S and chalcophile element (such as Cu) inventory of the martian mantle.

Martian mantle heterogeneity and S-Cu abundance constraints

Although evidence exists for past mantle overturn[75,76] and potential present-day convection[77], the $\delta^{65}Cu$ heterogeneity in martian mantle-derived materials suggests preservation of ITE-enriched reservoirs.

https://doi.org/10.1038/s41467-025-64331-z

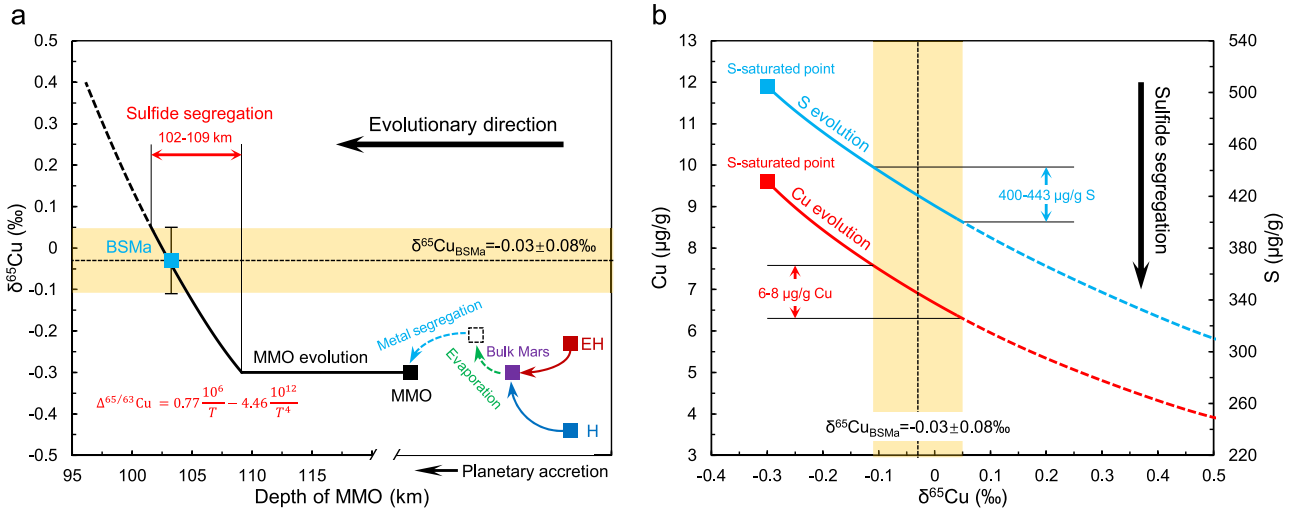

Fig. 5 | Martian evolutionary signatures recorded in δ^{65}Cu. Dashed lines in panels **a** and **b** represent extrapolated trends, assuming continued sulfide segregation during martian magma ocean (MMO) evolution. The bulk Mars was modeled as a mixture of 45% EH and 55% H chondrites[43], incorporating literature Cu abundances and isotopic data[2,8,11]. Copper sulfide-silicate isotopic fractionation coefficients ($\Delta^{65/63}$Cu) were parameterized following Xia et al. [3]. The error bar for BSMa represents 2 SD of representative samples. **a** Progressive enrichment in heavy isotopes (δ^{65}Cu from −0.30‰ to +0.05‰) reflects the history of sulfide segregation. An inflection point at 109 km depth marks the onset of sulfide saturation, while the δ^{65}Cu upper limit of BSMa indicates the effective percolation threshold of sulfide melts at 102 km depth. **b** Systematic covariation between Cu-S depletion and δ^{65}Cu in residual melts (values converted to BSMa averages) results from variations in the extent of sulfide segregation.

Additionally, isotopic constraints (Re-Os in shergottites[78,79] and Sm-Nd/Lu-Hf in regolith breccia NWA 7034[25]) challenge the interpretation that martian crust is the dominant source of shergottite ITE-enriched components. If validated by further evidence, this perspective would imply that such ITE-enriched mantle domains represent a primary source of ITE-enriched components. Critically, the persistence of these localized mantle reservoirs indicates inefficient martian mantle convection (Fig. 4d). Within this framework, the mantle S-Cu abundances defined for BSMa therefore likely reflect the composition of the broader ITE-depleted mantle.

Building upon the constraints provided by Cu isotopes, our model estimates a martian mantle Cu abundance of 6–8 μg/g (Fig. 5b). Although our estimate for the mantle is higher than previous meteorite-based inversions (2–3 μg/g[19,80,81]), both estimates fall within the same order of magnitude. Our model also yields a core concentration of ~354 μg/g, which is slightly lower than the previous estimate of ~560 μg/g[81]. For sulfur, we estimate a mantle content of 400–443 μg/g (Fig. 5b; upper limit without accounting for evaporation losses), consistent with sulfur-poor mantle models (e.g., 360 ± 120 μg/g[19] and 200–450 μg/g[18]) but significantly lower than sulfur-rich proposals (2000–2200 μg/g[82] and a maximum of 1000 μg/g[83]). The discrepancies between our estimates and previous work potentially stem from our different approach, which uses cosmochemical constraints derived from integrating accretionary parameters and Cu isotopes, whereas prior studies relied predominantly on geochemical inversions[19,80–83]. Critically, our model suggests that sulfide segregation during MMO crystallization further reduced the mantle inventories of chalcophile elements, which is inconsistent with sulfur-rich mantle models. This depletion is consistent with the core's sulfur-rich signature (~16.1 wt.%, within the reported range of 3.5–25 wt.%[42,43,80,81,84–87]). Together, this sulfur-rich core and sulfur-poor mantle configuration reflect the efficient sequestration of S and chalcophile elements into the core during planetary differentiation. Consequently, the mantle's depletion in S provides a key explanation for the suppression of sulfide saturation in derivative magmas.

Notably, our model neglects the potential contribution of interstitial melts retained during crystallization. Although compaction likely expelled most melt from the solidifying cumulates, trapped intergranular melts could add incompatible elements to ITE-depleted mantle domains. Owing to uncertainties in quantifying solid compaction efficiency during MMO evolution, the estimated S and Cu abundances in the martian mantle should be considered approximate. Nevertheless, by using the martian differentiation model to constrain mantle S-Cu abundances with δ^{65}Cu, this study highlights the important role of sulfide segregation in controlling global-scale distributions of chalcophile elements.

Methods

Sample description and analytical preparation

Samples were obtained from meteorite dealers. The analyzed martian meteorites include 13 shergottites and two nakhlites (Table 1), all classified as igneous rocks. Except for the witnessed fall Zagami, all specimens were recovered as hot desert finds. Optical and electron microscopy observations revealed minimal evidence of terrestrial weathering in most samples (Supplementary Figs. 1–11 for representative images). However, some samples (e.g., NWA 6963; Supplementary Fig. 13) exhibited terrestrial contamination features, including trace amounts of terrestrial carbonates.

Before chemical and isotopic analysis, visually contaminated areas were manually removed, and samples were leached in 0.1 N HCl for 1 min to remove potential terrestrial weathering contaminants (particularly carbonates). The leached fragments were then pulverized into fine powders using an agate mortar for subsequent major/trace elements analyses and isotopic measurements. Additionally, NWA 13276 chip 2 was sampled from the weathered exterior portion of NWA 13276 chip 1 and was measured without acid leaching to specifically monitor terrestrial weathering effects.

Petrographic characterization

Petrographic analyses were conducted at the Center for Lunar and Planetary Sciences, Institute of Geochemistry, Chinese Academy of Sciences, using the FEI Scios-FIB field emission scanning electron microscope (SEM) equipped with energy dispersive spectrum (EDS). The beam accelerating voltage was 20 kV, and the beam current was 0.8 nA. Elemental mapping was performed using the TESCAN

Integrated Mineral Analyzer (TIMA) at the State Key Laboratory for Critical Mineral Research and Exploration, Institute of Geochemistry, Chinese Academy of Sciences. The TIMA system is equipped with an auto-scanning electron microscope (ASEM) and four EDS detectors. The beam accelerating voltage was 25 kV, and the beam current was 9.49 nA.

Elemental composition

Major and trace element concentrations were measured using a Thermo Fisher inductively coupled plasma mass spectrometry (ICP–MS) X2 at the Guizhou Tongwei Analytical Technology Co., Ltd. Details can be found in Li et al.[88]. Analytical accuracy was assessed via analyses of geostandard BCR-2. The relative standard deviations for duplicates are reported in Supplementary Data 1.

Chemical pretreatment

Copper purification was performed at the Isotope Geochemistry Laboratory, China University of Geosciences (Beijing), using the procedure of Liu et al.[89] modified from Maréchal et al.[90]. Samples containing ≥500 ng Cu were digested in distilled HF-HNO_3 (volume 1:1) at 130 °C for 48 h, dried, re-dissolved in aqua regia, and evaporated to dryness. The residues were dissolved in HCl, dried, and finally re-dissolved in 1 ml 8 N HCl with 0.001% H_2O_2 for column chemistry. The resulting solution was loaded into a column containing pre-cleaned AG-MP-1M resin (100–200 mesh) to separate Cu from the matrix. The column procedure was repeated twice (for a total of three cycles). Purified Cu solutions were dried and re-dissolved in 3% HNO_3 for isotopic analysis.

Copper isotopic analysis

Copper isotopic compositions were measured on a Thermo Scientific Neptune multi-collector inductively coupled plasma mass spectrometry (MC–ICP–MS) at the Isotope Geochemistry Laboratory, China University of Geosciences (Beijing). The sample-standard bracketing method was employed to correct for instrumental mass bias. The Cu isotopic compositions are reported as δ^{65}Cu relative to the standard reference material (SRM) NIST976: $\delta^{65}Cu=[(^{65}Cu/^{63}Cu)_{sample}/(^{65}Cu/^{63}Cu)_{NIST976}-1]\times1000$. Measurement uncertainties are reported as the long-term precision during the course of the measurement session, which is constrained to the 2 SD of the bracketed standard GSB-Cu. Each sample solution was measured three times. The internal precision (2 SD) of three-time measurements of each sample is usually lower than 0.04‰, and thus we report the long-term precision of each measurement session as the errors. Total Cu blank is <1 ng, which is negligible compared to ≥500 ng Cu loaded on the column. The GSB-Cu standard yielded a δ^{65}Cu value of +0.44 ± 0.04‰ relative to NIST 976[89]. Each sample was measured in three blocks of 40 cycles with an integration time of 4.194 s.

The alphaMELTS 1.9 simulation

MMO crystallization processes were modeled using alphaMELTS 1.9 software[68–70]. The initial simulation parameters were derived from our chemical and physical modeling of Mars (Supplementary Method 3), which referenced published studies[43,55,60,62,81,91–93] and incorporated mass balance calculations. This yielded parameters for bulk Mars, the BSMa, and the core (Supplementary Tables 1, 2). Owing to the limitations of the software in simulating crystallization above 3 GPa (MELTS mode), we used the residual melt from 24.4% partial melting of BSMa to approximate melt compositions at 75.6% crystallization, corresponding to a 3 GPa magma ocean. A batch melting model was employed, as magma ocean crystallization approximates equilibrium once residual melt fraction exceeds 20%[23,94]. This assumption reflects a predominantly convective magma ocean, in which suspended crystals remain in chemical equilibrium with the melt. This strategy circumvents uncertainties in high-pressure thermodynamical calculations. Simulations were initialized with the BSMa composition (major elements excluding S) for magma ocean crystallization, and theoretically no late-stage metal alloy exsolution. To suppress metal alloy formation, alphaMELTS 1.9 parameters were adjusted accordingly. The melt was simulated in 0.2 GPa pressure intervals under isobaric cooling to track temperature changes and crystallization progress. Each pressure step was modeled as equilibrium crystallization, with residual melt compositions from the previous step (i.e., manual fractional crystallization was applied between steps). Full computational settings and methodological workflows are provided in the Supplementary Data 3. Simulation outputs, including pressure-dependent crystallization fractions, solid and residual melt compositions, and melt liquidus temperatures, are summarized in Supplementary Data 4.

Data availability

All data generated or analyzed during this study are included in this published article (and its supplementary information files). The complete set of unprocessed raw raster images has been deposited in the figshare data repository under accession code (https://doi.org/10.6084/m9.figshare.29994751)[95]. Source data are provided with this paper.

Code availability

The alphaMELTS 1.9 software, used for modeling magma ocean crystallization, is available at https://magmasource.caltech.edu/alphamelts/. All customized command parameters for the alphaMELTS 1.9 simulations in this study are provided in Supplementary Data 3.

References

1. Righter, K. et al. Ag isotopic and chalcophile element evolution of the terrestrial and martian mantles during accretion: new constraints from Bi and Ag metal-silicate partitioning. *Earth Planet. Sci. Lett.* **552**, 116590 (2020).
2. Savage, P. S. et al. Copper isotope evidence for large-scale sulphide fractionation during Earth's differentiation. *Geochem. Perspect. Lett.* **1**, 53–64 (2015).
3. Xia, Y., Kiseeva, E. S., Wade, J. & Huang, F. The effect of core segregation on the Cu and Zn isotope composition of the silicate Moon. *Geochem. Perspect. Lett.* **12**, 12–17 (2019).
4. Neuman, M. et al. Volatile element evolution in the martian crust: communications with the martian surface and atmosphere? In *Proc. 53rd Lunar and Planetary Science Conference*. 1385 (Lunar and Planetary Institute, 2022).
5. Liu, S.-A. et al. Copper isotopic composition of the silicate Earth. *Earth Planet. Sci. Lett.* **427**, 95–103 (2015).
6. Paquet, M., Moynier, F., Sossi, P. A., Dai, W. & Day, J. M. D. Volatile loss history of the Moon from the copper isotopic compositions of mare basalts. *Earth Planet. Sci. Lett.* **656**, 119250 (2025).
7. Florin, G., Gleißner, P. & Becker, H. Copper isotopes in mare basalts reveal metal-silicate equilibration in the lunar magma ocean. *Geochim. Cosmochim. Acta* **402**, 372–387 (2025).
8. Luck, J. M., Othman, D. B., Barrat, J. A. & Albarède, F. Coupled ^{63}Cu and ^{16}O excesses in chondrites. *Geochim. Cosmochim. Acta* **67**, 143–151 (2003).
9. Barrat, J. A. et al. Geochemistry of CI chondrites: major and trace elements, and Cu and Zn isotopes. *Geochim. Cosmochim. Acta* **83**, 79–92 (2012).
10. Paquet, M. et al. Contribution of Ryugu-like material to Earth's volatile inventory by Cu and Zn isotopic analysis. *Nat. Astron.* **7**, 182–189 (2023).
11. Moynier, F., Blichert-Toft, J., Telouk, P., Luck, J.-M. & Albarède, F. Comparative stable isotope geochemistry of Ni, Cu, Zn, and Fe in chondrites and iron meteorites. *Geochim. Cosmochim. Acta* **71**, 4365–4379 (2007).

12. Ni, P., Macris, C. A., Darling, E. A. & Shahar, A. Evaporation-induced copper isotope fractionation: Insights from laser levitation experiments. *Geochim. Cosmochim. Acta* **298**, 131–148 (2021).
13. Day, J. M. D. et al. Moderately volatile element behaviour at high temperature determined from nuclear detonation. *Geochem. Perspect. Lett.* **13**, 54–60 (2020).
14. Udry, A. et al. What martian meteorites reveal about the interior and surface of Mars. *J. Geophys. Res. Planets* **125**, e2020JE006523 (2020).
15. Huang, J., Huang, F., Wang, Z., Zhang, X. & Yu, H. Copper isotope fractionation during partial melting and melt percolation in the upper mantle: evidence from massif peridotites in Ivrea-Verbano Zone, Italian Alps. *Geochim. Cosmochim. Acta* **211**, 48–63 (2017).
16. Lee Cin-Ty, A. et al. Copper systematics in arc magmas and implications for crust-mantle differentiation. *Science* **336**, 64–68 (2012).
17. Baumgartner, R. J. et al. The role of sulfides in the fractionation of highly siderophile and chalcophile elements during the formation of martian shergottite meteorites. *Geochim. Cosmochim. Acta* **210**, 1–24 (2017).
18. Paquet, M. et al. Highly siderophile elements in shergottite sulfides and the sulfur content of the martian mantle. *Geochim. Cosmochim. Acta* **293**, 379–398 (2021).
19. Wang, Z. & Becker, H. Chalcophile elements in martian meteorites indicate low sulfur content in the martian interior and a volatile element-depleted late veneer. *Earth Planet. Sci. Lett.* **463**, 56–68 (2017).
20. Blanchard, I., Abeykoon, S., Frost, D. J. & Rubie, D. C. Sulfur content at sulfide saturation of peridotitic melt at upper mantle conditions. *Am. Mineralogist* **106**, 1835–1843 (2021).
21. Blanchard, I. et al. Earth's deep magma ocean never reached sulfide saturation. *Geochem. Perspect. Lett.* **34**, 6–10 (2025).
22. Zhao, S.-Y., Yang, A. Y., Langmuir, C. H. & Zhao, T.-P. Oxidized primary arc magmas: constraints from Cu/Zr systematics in global arc volcanics. *Sci. Adv.* **8**, eabk0718 (2022).
23. Borg, L. E. & Draper, D. S. A petrogenetic model for the origin and compositional variation of the martian basaltic meteorites. *Meteorit. Planet. Sci.* **38**, 1713–1731 (2003).
24. Debaille, V., Brandon, A. D., Yin, Q. Z. & Jacobsen, B. Coupled ^{142}Nd–^{143}Nd evidence for a protracted magma ocean in Mars. *Nature* **450**, 525–528 (2007).
25. Armytage, R. M. G., Debaille, V., Brandon, A. D. & Agee, C. B. A complex history of silicate differentiation of Mars from Nd and Hf isotopes in crustal breccia NWA 7034. *Earth Planet. Sci. Lett.* **502**, 274–283 (2018).
26. Debaille, V., Yin, Q. Z., Brandon, A. D. & Jacobsen, B. Martian mantle mineralogy investigated by the ^{176}Lu–^{176}Hf and ^{147}Sm–^{143}Nd systematics of shergottites. *Earth Planet. Sci. Lett.* **269**, 186–199 (2008).
27. Lapen, T. J. et al. Two billion years of magmatism recorded from a single Mars meteorite ejection site. *Sci. Adv.* **3**, e1600922 (2017).
28. Humayun, M. et al. Origin and age of the earliest martian crust from meteorite NWA7533. *Nature* **503**, 513–516 (2013).
29. Agee, C. B. et al. Unique meteorite from early Amazonian Mars: water-rich basaltic breccia Northwest Africa 7034. *Science* **339**, 780–785 (2013).
30. Liu, S.-A. et al. Copper isotope evidence for sulfide fractionation and lower crustal foundering in making continental crust. *Sci. Adv.* **9**, eadg6995 (2023).
31. Zhang, T. et al. Copper and Zinc isotope signatures in scleratinian corals: Implications for Cu and Zn cycling in modern and ancient ocean. *Geochim. Cosmochim. Acta* **317**, 395–408 (2022).
32. Qu, Y.-R. & Liu, S.-A. Copper isotope constraints on the origins of basaltic and andesitic magmas in the Tengchong volcanic field, SE Tibet. *Geosci. Front.* **15**, 101818 (2024).
33. Le Roux, V., Dasgupta, R. & Lee, C. T. A. Mineralogical heterogeneities in the Earth's mantle: constraints from Mn, Co, Ni and Zn partitioning during partial melting. *Earth Planet. Sci. Lett.* **307**, 395–408 (2011).
34. Day, J. M. D. Metal grains in lunar rocks as indicators of igneous and impact processes. *Meteorit. Planet. Sci.* **55**, 1793–1807 (2020).
35. Li, Y. & Audétat, A. Effects of temperature, silicate melt composition, and oxygen fugacity on the partitioning of V, Mn, Co, Ni, Cu, Zn, As, Mo, Ag, Sn, Sb, W, Au, Pb, and Bi between sulfide phases and silicate melt. *Geochim. Cosmochim. Acta* **162**, 25–45 (2015).
36. Sun, P. et al. Copper isotope fractionation during magma differentiation: evidence from lavas on the East Pacific Rise at 10°30'N. *Geochim. Cosmochim. Acta* **356**, 93–104 (2023).
37. Udry, A. & Day, J. M. D. 1.34 billion-year-old magmatism on Mars evaluated from the co-genetic nakhlite and chassignite meteorites. *Geochim. Cosmochim. Acta* **238**, 292–315 (2018).
38. Treiman, A. H. The nakhlite meteorites: Augite-rich igneous rocks from Mars. *Geochemistry* **65**, 203–270 (2005).
39. McCubbin, F. M. et al. A petrogenetic model for the comagmatic origin of chassignites and nakhlites: Inferences from chlorine-rich minerals, petrology, and geochemistry. *Meteorit. Planet. Sci.* **48**, 819–853 (2013).
40. Day, J. M. D. et al. Martian magmatism from plume metasomatized mantle. *Nat. Commun.* **9**, 4799 (2018).
41. Daly, L. et al. Boom boom pow: Shock-facilitated aqueous alteration and evidence for two shock events in the martian nakhlite meteorites. *Sci. Adv.* **5**, eaaw5549 (2019).
42. Lodders, K. & Fegley, B. An oxygen isotope model for the composition of Mars. *Icarus* **126**, 373–394 (1997).
43. Sanloup, C., Jambon, A. & Gillet, P. A simple chondritic model of Mars. *Phys. Earth Planet. Inter.* **112**, 43–54 (1999).
44. Dauphas, N., Hopp, T. & Nesvorný, D. Bayesian inference on the isotopic building blocks of Mars and Earth. *Icarus* **408**, 115805 (2024).
45. Burkhardt, C. et al. Terrestrial planet formation from lost inner solar system material. *Sci. Adv.* **7**, eabj7601 (2021).
46. Kleine, T., Steller, T., Burkhardt, C. & Nimmo, F. An inner solar system origin of volatile elements in Mars. *Icarus* **397**, 115519 (2023).
47. Paquet, M., Sossi, P. A. & Moynier, F. Origin and abundances of volatiles on Mars from the zinc isotopic composition of martian meteorites. *Earth Planet. Sci. Lett.* **611**, 118126 (2023).
48. Dhaliwal, J. K., Day, J. M. D., Creech, J. B. & Moynier, F. Copper and zinc isotope compositions of pristine eucrites as analogues for differentiated planetary feedstocks. *Earth Planet. Sci. Lett.* **637**, 118740 (2024).
49. Kruijer, T. S. et al. The early differentiation of Mars inferred from Hf–W chronometry. *Earth Planet. Sci. Lett.* **474**, 345–354 (2017).
50. Halliday, A. N. & Canup, R. M. The accretion of planet Earth. *Nat. Rev. Earth Environ.* **4**, 19–35 (2023).
51. Davies, E. J. et al. Silicate melting and vaporization during rocky planet formation. *J. Geophys. Res. Planets* **125**, e2019JE006227 (2020).
52. Johansen, A. et al. A pebble accretion model for the formation of the terrestrial planets in the Solar System. *Sci. Adv.* **7**, eabc0444 (2021).
53. Young, E. D. et al. Near-equilibrium isotope fractionation during planetesimal evaporation. *Icarus* **323**, 1–15 (2019).
54. Sossi, P. A. et al. An experimentally-determined general formalism for evaporation and isotope fractionation of Cu and Zn from silicate melts between 1300 and 1500°C and 1bar. *Geochim. Cosmochim. Acta* **288**, 316–340 (2020).
55. Wasson, J. T., Kallemeyn, G. W., Runcorn, S. K., Turner, G. & Woolfson, M. M. Compositions of chondrites. *Philos. Trans. R. Soc. Lond. Ser. A Math. Phys. Sci.* **325**, 535–544 (1988).
56. Hu, Y., Moynier, F. & Bizzarro, M. Potassium isotope heterogeneity in the early Solar System controlled by extensive evaporation and partial recondensation. *Nat. Commun.* **13**, 7669 (2022).

57. Tian, Z. et al. Potassium isotope composition of Mars reveals a mechanism of planetary volatile retention. *Proc. Natl Acad. Sci.* **118**, e2101155118 (2021).
58. O'Neill, H. S. C. The origin of the moon and the early history of the earth—A chemical model. Part 2: The Earth. *Geochim. Cosmochim. Acta* **55**, 1159–1172 (1991).
59. Righter, K. & Chabot, N. L. Moderately and slightly siderophile element constraints on the depth and extent of melting in early Mars. *Meteorit. Planet. Sci.* **46**, 157–176 (2011).
60. Rai, N. & van Westrenen, W. Core-mantle differentiation in Mars. *J. Geophys. Res. Planets* **118**, 1195–1203 (2013).
61. Yang, S. et al. Siderophile and chalcophile element abundances in shergottites: Implications for martian core formation. *Meteorit. Planet. Sci.* **50**, 691–714 (2015).
62. Suer, T.-A., Siebert, J., Remusat, L., Menguy, N. & Fiquet, G. A sulfur-poor terrestrial core inferred from metal–silicate partitioning experiments. *Earth Planet. Sci. Lett.* **469**, 84–97 (2017).
63. Mahan, B. et al. Investigating Earth's formation history through copper and sulfur metal-silicate partitioning during core-mantle differentiation. *J. Geophys. Res. Solid Earth* **123**, 8349–8363 (2018).
64. Wang, W. et al. Sulfur isotopic signature of Earth established by planetesimal volatile evaporation. *Nat. Geosci.* **14**, 806–811 (2021).
65. Hirschmann, M. M., Bergin, E. A., Blake, G. A., Ciesla, F. J. & Li, J. Early volatile depletion on planetesimals inferred from C–S systematics of iron meteorite parent bodies. *Proc. Natl Acad. Sci.* **118**, e2026779118 (2021).
66. Goldstein, J. I., Scott, E. R. D. & Chabot, N. L. Iron meteorites: crystallization, thermal history, parent bodies, and origin. *Geochemistry* **69**, 293–325 (2009).
67. Walker, R. J. et al. Modeling fractional crystallization of group IVB iron meteorites. *Geochim. Cosmochim. Acta* **72**, 2198–2216 (2008).
68. Smith, P. M. & Asimow, P. D. Adiabat_1ph: a new public front-end to the MELTS, pMELTS, and pHMELTS models. *Geochem. Geophys. Geosyst.* **6**, Q02004 (2005).
69. Ghiorso, M. S. & Sack, R. O. Chemical mass transfer in magmatic processes IV. A revised and internally consistent thermodynamic model for the interpolation and extrapolation of liquid-solid equilibria in magmatic systems at elevated temperatures and pressures. *Contrib. Mineral. Petrol.* **119**, 197–212 (1995).
70. Asimow, P. D. & Ghiorso, M. S. Algorithmic modifications extending MELTS to calculate subsolidus phase relations. *Am. Mineralogist* **83**, 1127–1132 (1998).
71. Laurenz, V., Rubie, D. C., Frost, D. J. & Vogel, A. K. The importance of sulfur for the behavior of highly-siderophile elements during Earth's differentiation. *Geochim. Cosmochim. Acta* **194**, 123–138 (2016).
72. ZhangZhou, J. et al. Predicting sulfide precipitation in magma oceans on Earth, Mars and the Moon using machine learning. *Geochim. Cosmochim. Acta* **366**, 237–249 (2024).
73. Wang, L. & Fei, Y. A partially equilibrated initial mantle and core indicated by stress-induced percolative core formation through a bridgmanite matrix. *Sci. Adv.* **9**, eade3010 (2023).
74. Kiseeva, E. S. & Wood, B. J. The effects of composition and temperature on chalcophile and lithophile element partitioning into magmatic sulphides. *Earth Planet. Sci. Lett.* **424**, 280–294 (2015).
75. Bouvier, L. C. et al. Evidence for extremely rapid magma ocean crystallization and crust formation on Mars. *Nature* **558**, 586–589 (2018).
76. Elkins-Tanton, L. T., Parmentier, E. M. & Hess, P. C. Magma ocean fractional crystallization and cumulate overturn in terrestrial planets: implications for Mars. *Meteorit. Planet. Sci.* **38**, 1753–1771 (2003).
77. Kiefer, W. S. & Li, Q. Water undersaturated mantle plume volcanism on present-day Mars. *Meteorit. Planet. Sci.* **51**, 1993–2010 (2016).
78. Brandon, A. D., Walker, R. J., Morgan, J. W. & Goles, G. G. Re-Os isotopic evidence for early differentiation of the martian mantle. *Geochim. Cosmochim. Acta* **64**, 4083–4095 (2000).
79. Brandon, A. D. et al. Evolution of the martian mantle inferred from the ^{187}Re–^{187}Os isotope and highly siderophile element abundance systematics of shergottite meteorites. *Geochim. Cosmochim. Acta* **76**, 206–235 (2012).
80. Taylor, G. J. The bulk composition of Mars. *Geochemistry* **73**, 401–420 (2013).
81. Yoshizaki, T. & McDonough, W. F. The composition of Mars. *Geochim. Cosmochim. Acta* **273**, 137–162 (2020).
82. Gaillard, F., Michalski, J., Berger, G., McLennan, S. M. & Scaillet, B. Geochemical reservoirs and timing of sulfur cycling on Mars. *Space Sci. Rev.* **174**, 251–300 (2013).
83. Ding, S., Dasgupta, R., Lee, C.-T. A. & Wadhwa, M. New bulk sulfur measurements of martian meteorites and modeling the fate of sulfur during melting and crystallization – Implications for sulfur transfer from martian mantle to crust–atmosphere system. *Earth Planet. Sci. Lett.* **409**, 157–167 (2015).
84. Wänke, H., Dreibus, G. & Wright, I. P. Chemistry and accretion history of Mars. *Philos. Trans. R. Soc. Lond. Ser. A Phys. Eng. Sci.* **349**, 285–293 (1994).
85. Morgan, J. W. & Anders, E. Chemical composition of Mars. *Geochim. Cosmochim. Acta* **43**, 1601–1610 (1979).
86. Ohtani, E. & Kamaya, N. The geochemical model of Mars: an estimation from the high pressure experiments. *Geophys. Res. Lett.* **19**, 2239–2242 (1992).
87. Khan, A. & Connolly, J. A. D. Constraining the composition and thermal state of Mars from inversion of geophysical data. *J. Geophys. Res. Planets* **113**, E07003 (2008).
88. Li, S. et al. Exposure history, petrology, and shock-induced sulfidization reaction of Alatage Mountain 001 strewn field samples. *Meteorit. Planet. Sci.* **56**, 1293–1310 (2021).
89. Liu, S.-A. et al. High-precision copper and iron isotope analysis of igneous rock standards by MC-ICP-MS. *J. Anal. At. Spectrom.* **29**, 122–133 (2014).
90. Maréchal, C. N., Télouk, P. & Albarède, F. Precise analysis of copper and zinc isotopic compositions by plasma-source mass spectrometry. *Chem. Geol.* **156**, 251–273 (1999).
91. Stähler, S. C. et al. Seismic detection of the martian core. *Science* **373**, 443–448 (2021).
92. Verhoeven, O. et al. Interior structure of terrestrial planets: modeling Mars' mantle and its electromagnetic, geodetic, and seismic properties. *J. Geophys. Res. Planets* **110**, E04009 (2005).
93. Bercovici, H. L., Elkins-Tanton, L. T., O'Rourke, J. G. & Schaefer, L. The effects of bulk composition on planetesimal core sulfur content and size. *Icarus* **380**, 114976 (2022).
94. Snyder, G. A., Taylor, L. A. & Neal, C. R. A chemical model for generating the sources of mare basalts: Combined equilibrium and fractional crystallization of the lunar magmasphere. *Geochim. Cosmochim. Acta* **56**, 3809–3823 (1992).
95. Wang, D.-L. Raw image data of martian differentiation history inferred from copper isotopes. figshare https://doi.org/10.6084/m9.figshare.29994751 (2025).
96. Moynier, F., Vance, D., Fujii, T. & Savage, P. The isotope geochemistry of zinc and copper. *Rev. Mineral. Geochem.* **82**, 543–600 (2017).
97. Sun, S. -s & McDonough, W. F. Chemical and isotopic systematics of oceanic basalts: implications for mantle composition and processes. *Geol. Soc. Lond. Spec. Publ.* **42**, 313–345 (1989).

Acknowledgements

The authors thank De-Han Shen, Lie-Meng Chen, Yu-Wei Zhang, Ming-Yang Li, Zhong-Sha Meng, and Qing-Wen Zhang for their suggestions. We are particularly grateful to Yun-Feng Du for his assistance with laboratory work. This study was financially supported by the National Key Research and Development Program of China (2022YFF0503100 to Jian-Zhong Liu and 2024YFF0807500 to Dan Zhu), the National

Natural Science Foundation of China (42373020 to Ying-Kui Xu, 42173046 to Shi-Jie Li, and 42073062 to Dan Zhu), the Pre-research Project on Civil Aerospace Technologies (D020202 to Dan Zhu), the Project of High-level Innovative Talents of Guizhou Province (GCC [2022] 017-1 to Shi-Jie Li), the Fundamental Research Funds for the Central Universities (2652023001 to Shui-Jiong Wang), and the Strategic Priority Research Program of the Chinese Academy of Sciences (XDA0430303 to Dan Zhu).

Author contributions

D.-L.W. and Y.-K.X. designed the project. Y.-K.X., S.-J.L. and Y.L. acquired the samples. D.-L.W., S.-J.W. and Z.-R.L. processed the samples and measured the Cu isotopic compositions. D.-L.W. conducted the petrographic analysis. D.Z. and D.-L.W. analyzed the datasets and conceptualized the model. D.-L.W. performed the model and drafted the initial manuscript with discussions from D.Z., Y.-K.X., S.-J.W., S.-J.L., Z.-R.L., Y.L., Z.L., H.T., X.-Y.L. and J.-Z.L.

Competing interests

The authors declare no competing interests.

Additional information

Supplementary information The online version contains supplementary material available at https://doi.org/10.1038/s41467-025-64331-z.

Correspondence and requests for materials should be addressed to Ying-Kui Xu or Shi-Jie Li.

Peer review information *Nature Communications* thanks Paul Savage, Pu Sun, and the other, anonymous, reviewer for their contribution to the peer review of this work. A peer review file is available.